JOURNAL OF SOLID STATE CHEMISTRY 115, 43–54 (1995)

A Modulation Wave Approach to Understanding the Disordered Structure of Cubic Stabilized Zirconias (CSZs)

T. R. Welberry, R. L. Withers, and S. C. Mayo

Research School of Chemistry, Australian National University, GPO Box 4, Canberra City, Australian Capital Territory 0200, Australia

Received March 14, 1994; accepted July 7, 1994

A computer model of the distribution of oxygen vacancies in a cubic stabilized zirconia (CSZ) has been directly synthesized by applying modulation waves to the fluorite-type *average* structure. Only waves having wave vectors defined by circles centered at the $\frac{1}{2}\{111\}^*$ reciprocal positions and in planes normal to the $\{111\}^*$ reciprocal directions were used for the synthesis. The derived oxygen-vacancy distribution was then used in conjunction with a previously reported method of applying cation relaxations to obtain computed diffraction patterns for comparison with the observed X-ray data. When the quantity modulated was taken as the occupancy of individual oxygen sites, the calculated diffraction patterns were unsatisfactory. However when the modulations were applied to $\frac{1}{2}\langle 111\rangle$ pairs of sites in each of four different orientations within the cube surrounding each cation site, the calculated diffraction patterns showed good qualitative agreement with the form of the observed patterns. The results of the study suggest a mechanism for the formation of the complex disordered structure. It is suggested that vacancy pairs oriented along a given $\langle 111\rangle$ direction produce a strain field that extends to large distances in the plane normal to that direction so that like-oriented vacancy pairs repel each other. In contrast, unlike-oriented vacancy pairs do not interact strongly. Rings of diffuse intensity of different radii and different degrees of diffuseness may be interpreted in terms of the amount of strain induced by such vacancy-pair defects and the concentration of defects demanded by the composition.

1. INTRODUCTION

The structure of pure zirconia, ZrO_2, is monoclinic at room temperature but is cubic at temperatures between ~2370°C and the melting point at ~2680°C. This high temperature phase can be "stabilized" to exist at room temperature via the addition of a relatively large amount (~5–50 mole%) of the oxides of a variety of lower valent metals such as CaO, MgO, Y_2O_3 and subsequent quench ing at ~1600°C. The anion-deficient materials that result have important ceramic and superionic conduction properties and are known collectively as cubic stabilized zirconias (or CSZs). Although the average structure of these materials is the simple fluorite-type structure (Space group $Fm3m$, with four cations and eight oxygen sites per unit cell—see Fig. 1), the question of exactly how the cations and the anions are arranged in detail has occupied numerous scientists over many years, and is still the subject of much debate (1–7).

Recently we reported a study of an yttria stabilized zirconia ($Zr_{0.61}Y_{0.39}O_{1.805}$) in which detailed diffuse X-ray scattering measurements were made of several sections through the three-dimensional diffraction pattern of the material (8, 9). These data, recorded on a position-sensitive detector system, revealed a level of detail hitherto unavailable, and this allowed a viable model to be proposed for the complex disordered structure. The model consists of two stages; use of a near-neighbor vacancy–vacancy interaction potential to induce ordering of the oxygen vacancies, followed by use of an algorithm to allow the cation positions to relax around these vacancy sites. The model, tested by Monte Carlo simulation, which (qualitatively) best fitted the observed patterns was one in which the vacancies ordered in such a way as to avoid nearest-neighbor, $\frac{1}{2}\langle 100\rangle$, and next-nearest $\frac{1}{2}\langle 110\rangle$ vacancy pairs as well as $\frac{1}{2}\langle 111\rangle$ pairs along the body diagonal of a cube of oxygens not containing a cation. $\frac{1}{2}\langle 111\rangle$ vacancy pairs in cubes containing cations were relatively favored, but these tended to occur mainly as isolated pairs or as short zigzag chains of no more than two or three pairs. The algorithm which was used to carry out the cation relaxation was one which moved nearest-neighbor, $\frac{1}{2}\langle 110\rangle$ cations further apart if either of the two bridging oxygen atom sites were vacant or relatively closer together otherwise. This study showed that the observed diffuse scattering could be almost entirely accounted for by the scattering due to the displacements of the cations. The actual short-range order (SRO) scattering due to the disordered oxygen distribution was found to be a relatively minor component of the total scattering. Because the atomic scattering factors for Zr and Y are very similar, SRO scattering due to the ordering of the cations was also not detectable.

Although this study was able to account satisfactorily for practically all of the diffuse scattering features observed in the particular Y–CSZ studied, a longer term

0022-4596/95 $6.00

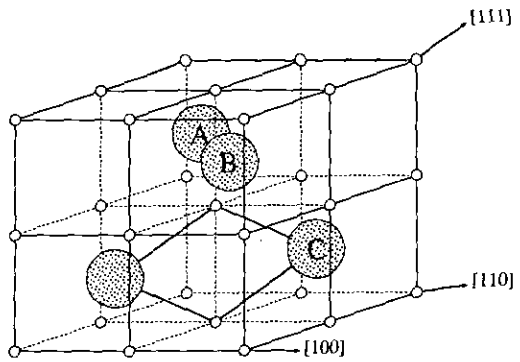

FIG. 1. Schematic diagram of the average unit cell of cubic stabilized zirconia. Small circles represent the oxygen array which contains vacancies and large shaded circles the cation array which is complete but disordered. The heavy lines indicate how a pair of oxygen sites forms a bridge between neighboring cation sites. There are chains of such bridged cations extending along the ⟨110⟩ directions. Note that cation sites labeled A, B, and C lie in a plane normal to [111].

aim of our present research is to try to understand the whole solid solution range of this and other different CSZs. So far data of a comparable quality have been collected from a Ca–CSZ and other data collections are in progress. For this Ca–CSZ material ($Zr_{0.875}Ca_{0.125}O_{1.875}$), the diffuse diffraction patterns contain much more sharply peaked features than in the Y–CSZ example, indicating a range of order that extends to much greater distances. Many features of the patterns are nevertheless very similar, suggesting the basic ordering mechanism is the same. (Some example sections of the Ca–CSZ data together with the corresponding sections of the Y–CSZ data are reproduced for comparison in Figs. 2a–2d.) Attempts to modify the simple vacancy ordering scheme used for the Y–CSZ to induce ordering over this extended range have so far been unsuccessful. The aim of the present work therefore is to use a quite different approach to the problem of disorder in CSZ's in order to obtain more insight into the possible mechanisms for the vacancy ordering.

The use of local interaction potentials and a description of the resulting structure in terms of correlations between occupancies and displacements of atoms may be termed a "real-space" description of a disordered system. An alternative, but in principle entirely equivalent, approach is the modulation-wave or "reciprocal-space" approach. In this the diffuse intensity occurring at any point in reciprocal space defined by the wave vector $\mathbf{G} + \mathbf{q}$, where $\mathbf{G}$ is a reciprocal lattice vector and $\mathbf{q}$ is a vector within the first Brillouin zone, can be considered to arise from a periodic perturbation of the real-space structure. For the case of concentration waves these perturbations can be written in the form of a variation from cell to cell of the atomic scattering factors, f_μ, where μ specifies an atomic site within the average unit cell. The modulation wave approach may generally be thought to be a more appropriate way of describing a disordered system in situations where the X-ray scattering pattern is highly structured and rather less so where only broad diffuse features are present (see Ref. 10). In the present case, although some CSZs do appear only to display very broad diffuse features, in others much sharper diffuse peaks are observed. In particular we were prompted to undertake the present investigation by the observation in electron diffraction patterns of some CSZs that the diffuse intensity appears to be confined to "rings" of intensity around the $\frac{1}{2}\{111\}$ reciprocal positions. Such rings may be simply defined by only two parameters, the radius and the width (diffuseness) of the ring. A typical electron diffraction pattern displaying these features is shown in Fig. 2e.

In the sections that follow we first give a brief description of the modulation wave approach to disorder and how it may be used to synthesize a real-space distribution. We then describe the application of the method to the problem of the distribution of the oxygen vacancies in CSZs. Finally we compare the results of this method with the previous Monte Carlo results.

THE MODULATION WAVE APPROACH

The diffuse intensity occurring at any point in reciprocal space defined by the wave vector $\mathbf{G} + \mathbf{q}$, where $\mathbf{G}$ is a reciprocal lattice vector and $\mathbf{q}$ is a vector within the first Brillouin zone, can be considered to arise from a periodic perturbation of the real-space structure. For the case of concentration waves these perturbations can be written in the form of a variation from cell to cell of the atomic scattering factors, f_μ, where μ specifies an atomic site within the average unit cell. That is, the scattering factor of the atom in the site μ of the unit cell with origin $\mathbf{T}$, where $\mathbf{T}$ is a real-space lattice vector, is given by

$$f_\mu(\mathbf{T}) = \langle f_\mu \rangle \left\{ 1 + \sum_{\mathbf{q}} A_{\mathbf{q}} \cos(2\pi \mathbf{q} \cdot \mathbf{T} + \phi_{\mu,\mathbf{q}}) \right\} \qquad [1]$$

The amplitude, $A_{\mathbf{q}}$, of each modulation wave is proportional to the amplitude of the scattering at the point $\mathbf{G} + \mathbf{q}$ in reciprocal space, and $\phi_{\mu,\mathbf{q}}$ is the phase of the modulation of wave vector $\mathbf{q}$ at the site μ. The summation is over all wave vectors in the first Brillouin zone.

Equation [1] may be used to *synthesize* a real-space distribution of atomic scattering factors which will have a given diffraction pattern. In simple terms the real-space lattice is constructed by applying modulations with wave vectors corresponding to each elemental volume in the first Brillouin zone of the diffraction pattern. Each modulation is given an amplitude which reflects the intensity at that point, and a phase that is chosen at random.

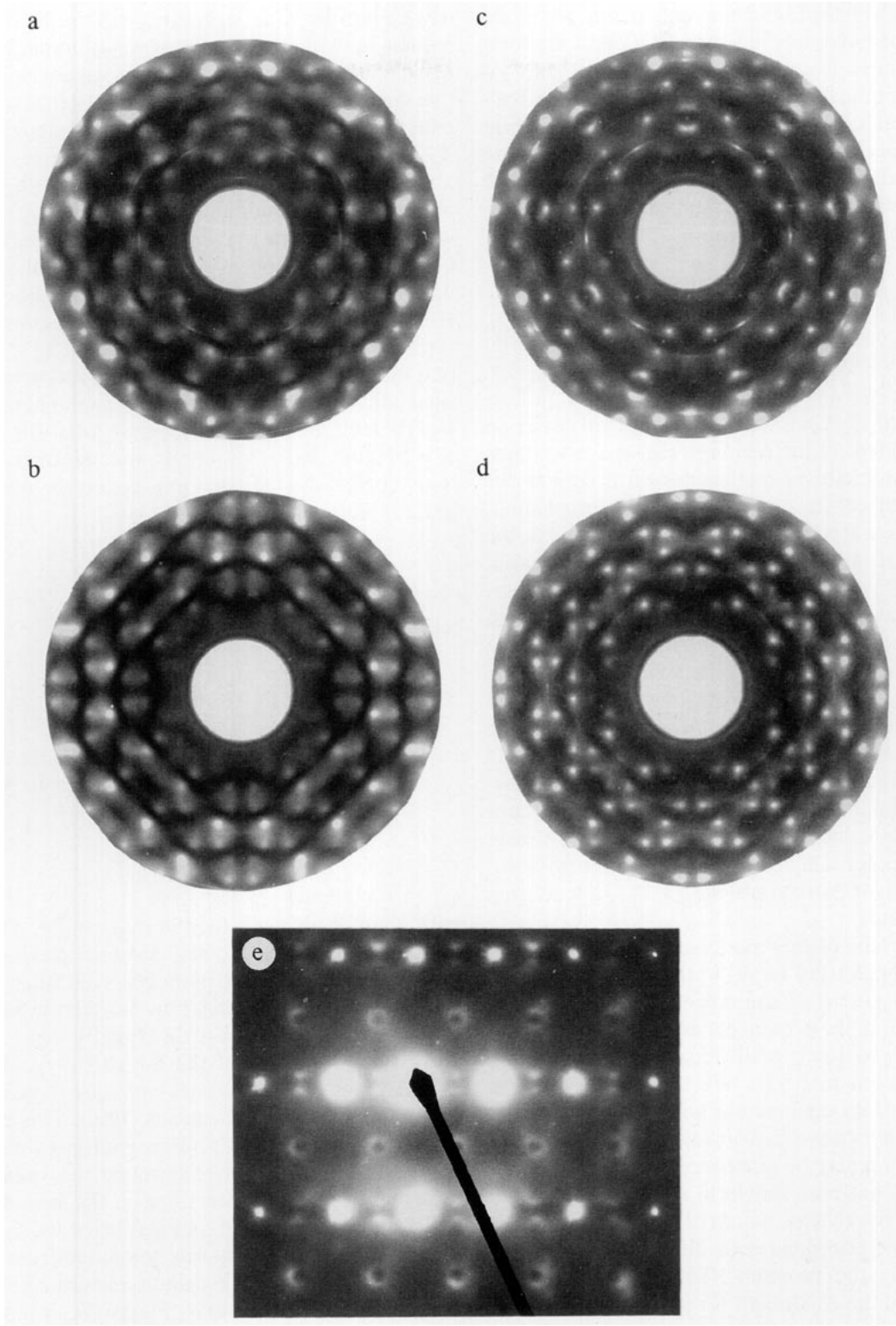

FIG. 2. Sections of the 3D diffuse X-ray diffraction patterns of yttria-stabilized cubic zirconia (a, b) and calcia-stabilized cubic zirconia (c, d). The sections are: (a, c) $h, k, l, h + k + l = 0.5$; (b, d), $h, k, 0.5$. The maximum value of the diffraction angle shown is ~117° of 2θ for Cu$K\alpha$ radiation. The sections were recorded using a position sensitive linear detector. The digital data are displayed as gray-scale images to facilitate visual comparison with the calculated patterns of Figs. 3 and 4. It should be noted however that no absorption correction has been applied to these data and this results in a relative diminution of intensity toward the centers of the figures. (e) shows an electron diffraction pattern of a terbium–CSZ ($Zr_{0.5}Tb_{0.5}O_{1.75}$) taken down the $[11\bar{2}]$ zone axis showing the diffuse circles discussed in the text.

In practice it has been found convenient, and computationally less expensive, to use a modification of the form of the modulations given in Eq. [1]. Whereas Eq. [1] implies that a modulation extends over the whole real-space structure and gives rise to intensity at a single point in reciprocal space, we consider instead a scheme where a modulation perturbs only a finite region of real-space and so gives rise to a more diffuse peak of intensity in reciprocal space. That is,

$$f_\mu(\mathbf{T}) = \langle f_\mu \rangle \left\{ 1 + \sum_{\mathbf{q}} A_{\mathbf{q}} \cos(2\pi \mathbf{q} \cdot \mathbf{T} + \phi_{\mu,\mathbf{q}}) \times \exp[-(\mathbf{t} - \mathbf{t}_c)^2 / 2\sigma_c^2] \right\}. \quad [2]$$

Here the final term is a Gaussian whose standard deviation σ_c defines the extent of the region in real-space which is perturbed; $\mathbf{t}$ is a vector in real space and $\mathbf{t}_c$ defines the randomly chosen center of the region of perturbation. The effect of such a perturbation is to contribute to the diffraction pattern a diffuse peak at the reciprocal point $\mathbf{q}$ with a width inversely proportional to σ_c.

If random phases $\phi_{\mu,\mathbf{q}}$ are used in the synthesis (and this is reasonable, since for an incommensurate wave the choice of origin is arbitrary) the value of the atomic scattering factor, $f_\mu(\mathbf{T})$, at a given site that will be obtained from Eq. [2] will be a continuous variable and not just a binary one (representing either atom A or atom B). This is overcome in practice by converting the continuous variables representing the scattering factors into binary ones by comparing the value of $f_\mu(\mathbf{T})$ with a threshold, f_T say. For all those sites for which $f_\mu(\mathbf{T}) > f_T$ a scattering factor f_A is assigned and for those at which $f_\mu(\mathbf{T}) \leq f_T$ a scattering factor f_B is assigned.

For further details of this modulation wave approach and how it has been used to aid in the interpretation of X-ray diffraction patterns of a number of different systems see Refs. (10–13). In the present paper we use this synthesis method to construct realizations of the oxygen-vacancy distribution in CSZs. We then, however, use these distributions in conjunction with the same cation relaxation procedure used previously, to obtain diffraction patterns which may be compared with the observed X-ray diffraction patterns shown in Fig. 2. In all of the examples in this paper, calculation of the diffraction patterns from atomic coordinates of different models was carried out using the program "Diffuse" (14) on the Fujitsu VP2200 at the Australian National University Supercomputer Facility.

MODULATION OF OXYGEN VACANCY CONCENTRATION

In this work, as for the previous study (9), an array of 64 × 64 × 64 oxygen sites (representing 32 × 32 × 32 unit cells of the CSZ structure) was used in the computer model. In the first experiment we attempted to construct a real-space distribution of oxygen vacancies on the primitive cubic lattice of 64 × 64 × 64 oxygen sites. The occupancy of any site u, v, w was represented by a variable $X_{u,v,w}$. Note that $\mathbf{T} \approx u\frac{1}{2}\mathbf{a}_1 + v\frac{1}{2}\mathbf{a}_2 + w\frac{1}{2}\mathbf{a}_3$ where $\mathbf{a}_1$, $\mathbf{a}_2$, $\mathbf{a}_3$ are the unit cell edges. The value of each $X_{u,v,w}$ was then obtained by summing over a large number of perturbing waves of the form [2]. Initially a value of $3.0 \times \frac{1}{2}\mathbf{a}$ was used for σ_c. A total of 3×10^5 individual perturbations were used. Assuming the perturbations have significant effect to a distance of $\pm 2.5\sigma_c$ this means that ~2000 perturbations contribute to each individual $X_{u,v,w}$. The values of $\mathbf{q}$ for the 3×10^5 individual perturbations were distributed uniformly around four circles centered on each of the $\frac{1}{2}\{111\}^*$ reciprocal positions. Noting that the unit vectors $1/\sqrt{2}\,(1\bar{1}0)^*$ and $1/\sqrt{6}\,(11\bar{2})^*$ are two orthogonal directions normal to [111], the expression for $\mathbf{q}$ on the circle radius r normal to [111] is

$$\mathbf{q} = h\mathbf{a}_1^* + \mathbf{k}\mathbf{a}_2^* + l\mathbf{a}_3^*$$

where

$$h = \frac{1}{2} + r\left[\frac{1}{\sqrt{2}}\cos(\theta) + \frac{1}{\sqrt{6}}\sin(\theta)\right]$$
$$k = \frac{1}{2} + r\left[-\frac{1}{\sqrt{2}}\cos(\theta) + \frac{1}{\sqrt{6}}\sin(\theta)\right] \quad [3]$$
$$l = \frac{1}{2} + r\left[-\frac{1}{\sqrt{6}}\sin(\theta)\right]$$

with θ uniformly covering the range 0–2π. The radius of the circle was chosen to be $0.3\mathbf{a}^*$ to correspond approximately with the distance of the pairs of diffuse peaks from the $\frac{1}{2}\{111\}^*$ positions, that may be seen in the observed diffraction patterns of Y-CSZ (Fig. 2).

By suitable choice of the threshold, f_T, the resulting $X_{u,v,w}$ were converted to binary values representing oxygen atoms (90%) and vacancies (10%). This binary array was then used as input to a program previously used to apply the cation distortions around the vacancies using the simple algorithm described in the introduction (see Ref. 9 for further details). In Figs. 3a–3c we show sections of the 3D diffraction patterns computed from the synthesized oxygen vacancy distribution and the resulting positions of the relaxed cations. Figure 3a shows the h, k, l, $h + k + l = 0.5$ section computed from the oxygen distribution itself. Clearly defined diffuse rings are seen in the section, but in addition pairs of peaks midway between two circles may also be seen. These peaks correspond to the intersection of this reciprocal section with circles normal to the other three $\langle 111 \rangle$ directions. This scattering

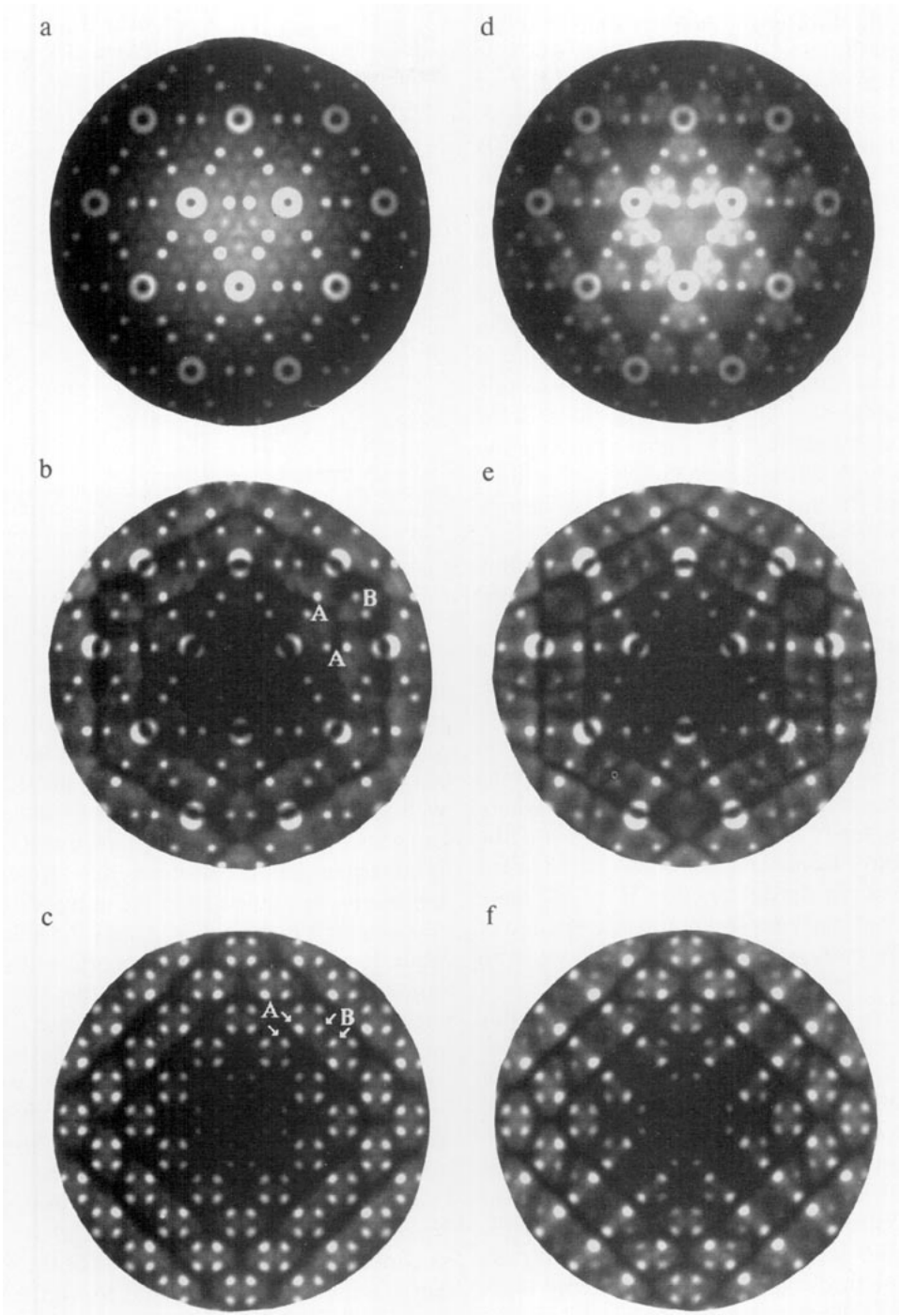

FIG. 3. Diffraction patterns calculated from two synthesized models. (a, b, c) correspond to a model in which modulations with wave vectors corresponding to all four orientations of the diffuse circles were applied to the basic primitive oxygen array. (d, e, f) correspond to the model in which modulations with wave vectors corresponding to each one orientation of diffuse circle were applied to the corresponding single orientation of the $\frac{1}{2}\langle 111\rangle$ pairs of oxygen sites surrounding a cation. (a, d) are the patterns calculated from the unperturbed oxygen distributions. (b, c, e, f) are calculated from cation displacements resulting from relaxation around the oxygen vacancies. The different sections are: (a, b, d, e) h, k, l, $h + k + l = 0.5$; (c, f) $h, k, 0.5$. For both sets of patterns the radius of the diffuse circle was $r = 0.3\mathbf{a}^*$ and the parameter specifying the diffuseness of the circle was $\sigma_c = 3.0 \times \frac{1}{2}\mathbf{a}$.

is proportional to the difference between the scattering factor for an oxygen (f_O) and that for a vacancy (=0), so is strong near the center and falls off toward the outside of the figure. Figures 3b and 3c by contrast were calculated using only the displacements of the cations induced by the relaxation algorithm. Here we have used the same scattering factor (f_{Zr}) for all cations. Figure 3b shows the pattern calculated for the same h, k, l, $h + k + l = 0.5$ section as shown in Fig. 3a. Figure 3c shows the corresponding h, k, 0.5 section. Although the lattice of cations is complete so there is no direct short-range order (SRO) scattering of the type seen in Fig. 3a, the pattern of their displacements around the oxygen vacancies clearly reflects the distribution of vacancies. In Fig. 3b both the in-plane diffuse circles and the pairs of peaks corresponding to sections through out-of-plane circles can still be seen. Now however the circles (and pairs of points) are intersected by the *dark-lines* which were shown in previous papers (9, 15) to be characteristic of the relaxation displacements. Similarly the transfer of intensity in the circles from the low-angle to the high-angle side of the dark lines is attributable to the fact that the cations move *away* from the vacancies and that the cation displacements are sufficiently large (~3%) to invoke third-order terms in the diffraction equation (see Refs. 16, 9). It should be noted that these two key features of the X-ray patterns are not so readily observed in electron diffraction where multiple diffraction tends to transfer intensity into the extinguished regions from translationally equivalent points in the pattern. In the $\frac{1}{2}\mathbf{c}^*$ section (Fig. 3c) quite distinct diffuse peaks clearly represent the intersection of all four of the differently oriented diffuse circles with this section.

Comparison of Figs. 3b and 3c with the corresponding sections of the observed data both for the Y–CSZ and for the Ca–CSZ shown in Fig. 2 clearly shows that this distribution of oxygen vacancies is quite wrong. The most obvious manifestation of the fact that the model is incorrect is in the azimuthal variation of the intensity of the diffuse peaks which arise from the intersection of the different circles. With references to the labeling of the peaks in Figs. 3b and 3c, it is clear that while the pairs of peaks "A" occur in the experimental patterns those labeled "B" do not. (They appear very weakly in the Ca–CSZ patterns, where in addition to scattering due to the displacements there will be a component due to SRO scattering.) Such azimuthal variation is caused by the *direction* of the displacements and it is clear from this that the displacements associated with the modulations of the oxygen concentration caused by wave vectors in the diffuse circle of one orientation must be quite distinct from those caused by wave vectors in circles of a different orientation. How can this be?

In the previous Monte Carlo work the model which qualitatively best accounted for the various features of the observed diffraction patterns was one in which the vacancies ordered in such a way as to avoid nearest-neighbor $\frac{1}{2}\langle 100\rangle$ and next-nearest $\frac{1}{2}\langle 110\rangle$ vacancy pairs as well as $\frac{1}{2}\langle 111\rangle$ pairs along the body diagonal of a cube of oxygens not containing a cation. But $\frac{1}{2}\langle 111\rangle$ vacancy pairs in cubes containing cations were relatively favored. These tendencies are reflected in the correlation coefficients between a given oxygen site and its neighbors which we reproduce in Table 1. Corresponding near-neighbor correlation values for the present synthesized array of oxygens are also given in Table 1. From these it is seen that none of the above conditions is satisfied by the present synthesized distribution. In the next section we describe a second synthesis in which instead of modulating the concentration of vacancies, we assume that the modulations refer to *pairs* of vacancies.

TABLE 1

Correlations between a Given Oxygen Site and Near-Neighboring Sites in the Fluorite Unit Cell of Different Models Discussed in the Text

Neighbor	Monte Carlo	Synthesis 1 $\sigma_c = 3.0 \times \mathbf{a}_1$	Synthesis 2 $\sigma_c = 3.0 \times \mathbf{a}_1$	Synthesis 2 $\sigma_c = 1.0 \times \mathbf{a}_1$
½[100]	−0.106	−0.000	−0.044	−0.041
½[100]	−0.106	−0.037	−0.058	−0.040
½[111][a]	−0.106	+0.000	−0.090	−0.062
½[111]	+0.336	+0.004	+0.260	+0.186
[100]	−0.067	−0.100	−0.074	−0.061
½[210]	+0.003	+0.001	−0.007	+0.009
½[211]	+0.030	+0.045	+0.024	+0.014
[110]	+0.006	+0.066	+0.035	+0.026
½[221]	−0.012	−0.001	+0.007	−0.011
[111]	−0.039	−0.011	−0.037	−0.009

Note. For a vacancy concentration of 0.10 the maximum negative correlation possible is −0.111. This value corresponds to the case where pairs of vacancies are completely avoided, but any negative value corresponds to a tendency to avoid pairs of vacancies separated by that particular vector. The values given are obtained by summing over all symmetry equivalent vectors in the cubic cell.
[a] Indicates a vector within a cube not occupied by a cation.

A final point to note from this first simulation is that the range of order produced by the use of $\sigma_c = 3.0 \times \frac{1}{2}\mathbf{a}$ is comparable to that observed for the Ca–CSZ example but for the Y–CSZ example the diffuse peaks are less pronounced and a much smaller value of σ_c is implied.

MODULATION OF THE CONCENTRATION OF OXYGEN VACANCY PAIRS

In this section we describe the synthesis of a distribution of oxygen vacancies on a lattice in which we try to ensure that vacancies occur in pairs along the body diagonal of cubes of oxygens which contain a cation (i.e., $\frac{1}{2}\langle 111\rangle$ pairs). Preservation of *local structure* in this way is not something which can easily be achieved by the synthesis

method and some approximations must be made. In the present case we make the following assumptions.

(i) We assume that the four $\frac{1}{2}\langle 111\rangle$ pairs of oxygen sites which make up the cube of oxygen sites surrounding each cation are each independent random variables.

(ii) We then assume that the distribution of the $\frac{1}{2}[111]$ pairs is caused only by modulations in the diffuse circle lying in a plane normal to [111]; that of the $\frac{1}{2}[11\bar{1}]$ pairs is caused only by modulations in the diffuse circle lying in a plane normal to $[11\bar{1}]$; etc.

(iii) If we assume ~10% vacancies overall, corresponding to the concentration of the Y–CSZ sample, then we assume that ~$2\frac{1}{2}$% occur in each of the four orientations. With this low concentration and the independence assumed for the four different orientations the probability that any one cation site will be associated with more than one vacancy pair will be extremely low (0.06%).

In Figs. 3d–3f we show diffraction patterns calculated from the distribution of vacancies synthesized by this new scheme. These were computed, after use of exactly the same cation relaxation algorithm, for comparison with the corresponding patterns from the first synthesis scheme shown in Figs. 3a–3c. The diffraction pattern calculated from the oxygens alone (Fig. 3d) appears very similar to that of Fig. 3a. Ideally if the concentration modulations are purely sinusoidal both these patterns should contain only the diffuse circles and pairs of spots that originate directly from the applied modulations. Other scattering features which can be seen, particularly towards the center of the pattern, arise from the conversion from the continuous variables to the binary variables which represent the concentration at a site. This conversion has the effect of generating higher harmonics of the basic modulations that have been imposed, and these represent a limitation of the method.

It should be noted in Fig. 3d that diffuse peaks corresponding to all four orientations of the diffuse circles are present, just as they were in Fig. 3a. In Fig. 3e, however, although superficially the pattern looks very similar to Fig. 3b, the peaks labeled "B" are absent. The effect is even more marked in Fig. 3f where the azimuthal variation of the different pairs of peaks is very obvious and much more like that of the experimental patterns.

It is interesting to compare the correlations between oxygen sites resulting from this second synthesis method. Correlation values for the near neighbor sites are given in the third column of Table 1. Now it is seen that strong negative correlations exist for each of the three types of neighboring pairs of sites; i.e., $\frac{1}{2}\langle 100\rangle$, $\frac{1}{2}\langle 110\rangle$, and $\frac{1}{2}\langle 111\rangle$ in cubes of oxygens not containing a cation, that were found to be important in the Monte Carlo model. The fact that we have introduced $\frac{1}{2}\langle 111\rangle$ pairs directly has resulted in a strong positive correlation for this vector. Since for a concentration of 0.1 the maximum negative correlation that can exist (corresponding to complete exclusion of vacancy pairs) is −0.111, it is clear that although the present synthesis has formed the same sort of local distribution as the Monte Carlo model, the extent of the exclusion of these types of vacancy pairs is by no means complete. It seems likely that the assumption that the distributions of the four different types of vacancy pairs are independent has contributed to this incompleteness, but a second likely contributor is the effect of higher harmonic generation caused by the conversion from real to binary variables discussed earlier.

In Figs. 4a–4c we show corresponding diffraction patterns computed from a synthesis identical to that described above, but for which the circles were much more diffuse. This was achieved with a value of $\sigma_c = 1.0 \times \frac{1}{2}\mathbf{a}$. In this synthesis 27 times more modulations were included to compensate for the reduced volume of real-space over which each significantly contributed. All other aspects of the two syntheses were the same. We show also in Figs. 4d–4f for comparison the corresponding patterns computed for the "best" Monte Carlo simulation reported previously. Qualitatively, these new patterns correspond very well to the observed patterns for Y–CSZ shown in Fig. 2. In most respects the agreement appears to be very similar to that shown by the previous Monte Carlo results but in some respects the new patterns may be even better. For example in Fig. 4c, there is more intensity in the broad flat regions of scattering marked "C" which spread between the pairs of diffuse peaks out in the [11] and $[1\bar{1}]$ directions from the origin.

The broad similarity between the synthesized distribution and the Monte Carlo model is also reflected in the values for the near-neighbor correlations given in Table 1. For all of the vectors listed the sign of the correlation (which essentially shows whether vacancy pairs separated by the given vector tend to be preferred or avoided) is the same. Generally speaking the correlations show that the synthesized distribution is attempting to make the same local configurations as the Monte Carlo simulation gave, but the "rules" dictating the avoidance of certain near-neighbor vacancy pairs are not being rigidly adhered to.

DISCUSSION OF REAL-SPACE STRUCTURE IMPLIED BY THE SYNTHESIS

The presence of diffuse circles in the diffraction patterns of CSZs may seem at first rather surprising, but in fact is not a particularly unusual feature. For example similar features are observed in the 3D diffraction patterns of the mineral mullite (17, 18). It is interesting to consider what exactly is implied by this circular distribution and what sort of atomic interactions may be causing it.

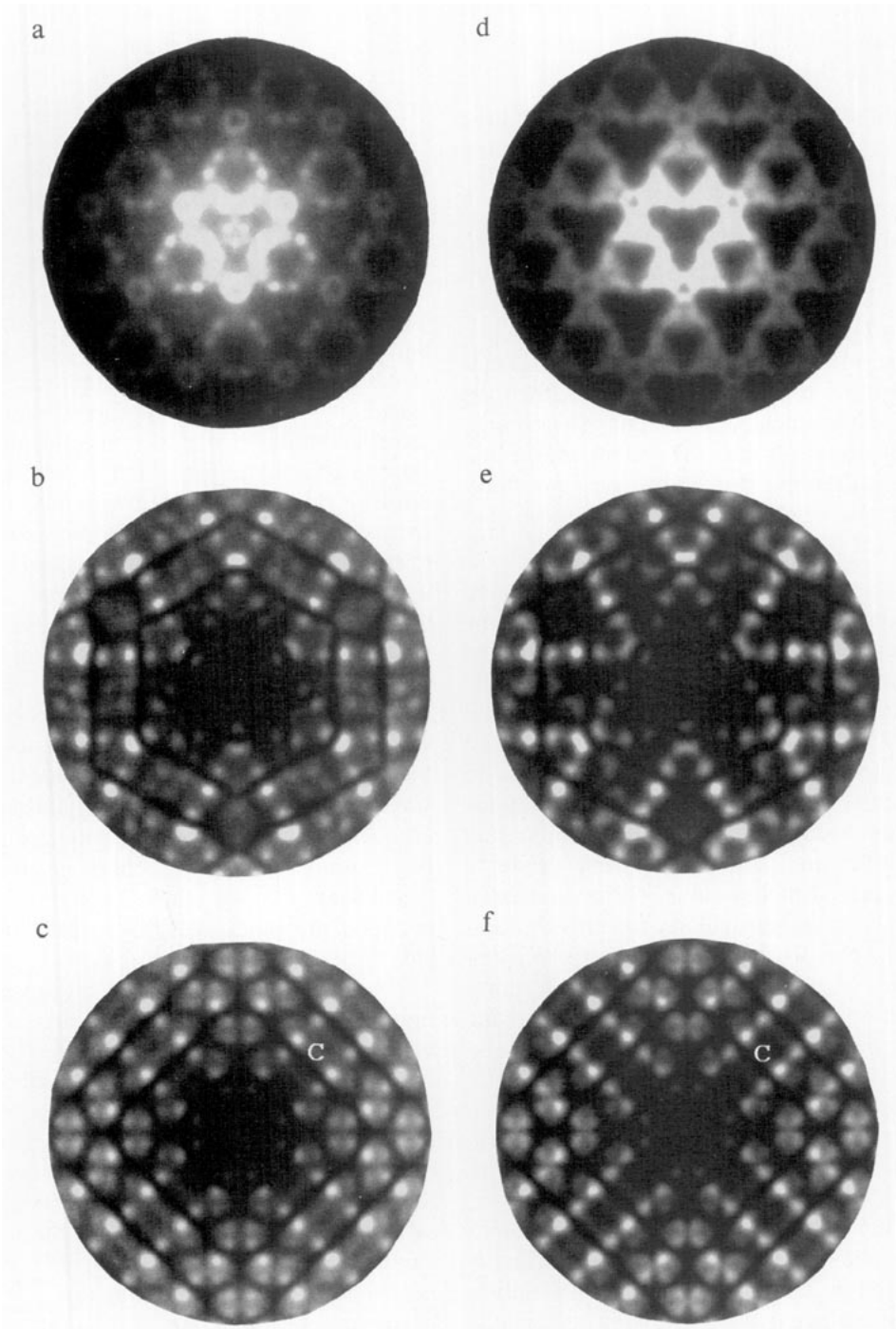

FIG. 4. Comparison of the diffraction patterns (a, b, c) calculated from a synthesized model with corresponding patterns (d, e, f) calculated from the "best" Monte Carlo model reported previously (9). (a, d) are the patterns calculated from the unperturbed oxygen distributions. (b, c, e, f) are calculated from cation displacements resulting from relaxation around the oxygen vacancies. The different sections are: (a, b, d, e) h, k, l, $h + k + l = 0.5$; (c, f) h, k, 0.5. For the synthesized model (a, b, c) the radius of the diffuse circle was $\rho = 0.3\mathbf{a}^*$ and the parameter specifying the diffuseness of the circle was $\sigma_c = 1.0 \times \frac{1}{2}\mathbf{a}$.

First let us consider modulations corresponding to only one of the four circle orientations, e.g., the circle normal to [111] defined by Eq. (3), and consider the real-space distribution in planes normal to [111]. In Fig. 5a we show a plot of a single layer of the cation sites of the CSZ structure synthesized using a value of $\sigma_c = 3.0 \times \frac{1}{2}\mathbf{a}$ and a circle radius, $r = 0.3\mathbf{a}^*$, as for the examples shown in Fig. 3. Here a black dot represents a cation site which is

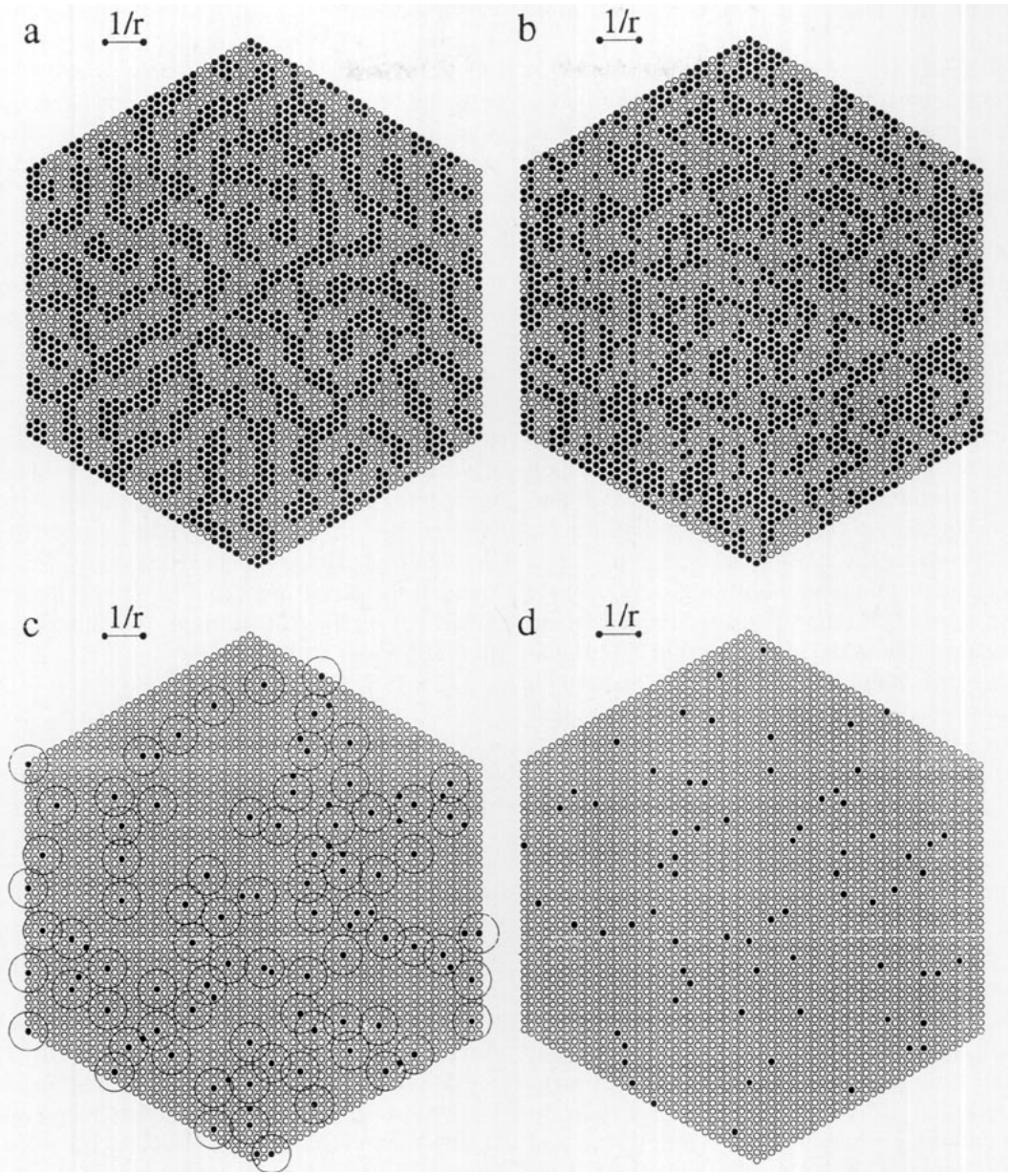

FIG. 5. Real-space distributions of cation sites in a (111) plane of CSZ obtained by the synthesis method described in the text. Black circles represent cation sites spanned by a $\frac{1}{2}[111]$ oxygen vacancy pair and white circles sites spanned by two occupied sites. (a, b) were synthesized using only wave vectors occurring in the diffuse circle in a plane normal to [111]. (c, d) are taken from the actual syntheses used to obtain the diffraction patterns of Figs. 3d–3f and 4a–4c respectively, in which wave vectors from all four circle orientations were used. For all four figures the radius of the diffuse circle was $r = 0.3\mathbf{a}^*$. The parameter specifying the diffuseness of the circle was $\sigma_c = 3.0 \times \frac{1}{2}\mathbf{a}$, for (a, c) and $\sigma_c = 1.0 \times \frac{1}{2}\mathbf{a}$, for (b, d).

spanned by a [111] vacancy pair and a white dot one which is not. For this plot the value of the conversion threshold was chosen to give 50% of vacancy pairs. The domains of black and white generated by this means have a very characteristic appearance of intermingled swirls, having an overall appearance which is quite isotropic. (See Ref. 19 for examples of the diffraction patterns of this kind of object.) The significance of the circle radius, r, can now be understood as it is the reciprocal of the mean spacing between neighboring black swirls. At the top left of the figure two additional black dots have been placed with a spacing corresponding to the reciprocal of r to help identify this characteristic distance. Because the diffuse circle occurs centered around $\frac{1}{2}(111)^*$, successive layers in the 3D structure are modulated out of phase and so the layer immediately below that shown has virtually the same

structure but with the black and white regions interchanged.

In the second figure (Fig. 5b) a similar distribution is shown, which has been synthesized, again using only one of the four circle orientations, but now with the value of $\sigma_c = 1.0 \times \frac{1}{2}\mathbf{a}$. Now, although the radius of the circle is the same and the average spacing between neighboring black regions reflects the same characteristic distance, the greater diffuseness of the circle means that there is more variation of the characteristic spacing.

Although the two figures described above provide some insight into the significance of the circles found in the diffraction patterns, the concentration of $\frac{1}{2}[111]$ vacancy pairs in a given layer in the syntheses which were used to model the real material is very much smaller (~2.5%). In Figs. 5c and 5d we show corresponding plots taken from the actual distributions from which Figs. 3d–3f and Figs. 4a–4c were calculated. Now we see that the vacancy pairs within this one layer are all isolated. The significance of the characteristic distance now only registers when it is realized that it represents a frequently occurring spacing between one vacancy pair and another nearby. To emphasize this we have drawn circles of diameter $1/r$ around a large fraction of the vacancy-pair sites and it is seen that these circles are all either in contact, almost in contact, or slightly overlapping. This constancy of inter-vacancy-pair distance is only really apparent for Fig. 5c for which $\sigma_c = 3.0 \times \frac{1}{2}\mathbf{a}$ since there is a much narrower spread of distances, but something of the same tendency must also be present in Fig. 5d.

In Fig. 5c in addition to a predominance of distances close to the characteristic length $1/r$, there are a number of much shorter inter-vacancy-pair spacings. Circles around the relatively small number of sites which result in these close contacts have been omitted. It seems likely that these extraneous sites exist because of the effect mentioned previously that conversion of the continuous to binary random variables inherent in the synthesis method induces higher harmonics of the basic modulations. Evidence for this is afforded by close scrutiny of Fig. 5c where it may be seen that nearly all of these extra points lie close to the periphery of other circles, indicating that they are close to a distance $1/2r$ from their neighbor.

If this explanation of the shorter inter-vacancy-pair spacings is accepted, then observation that the diffuse scattering tends to occur in "rings" around the $\{111\}^*$ directions may be interpreted as an attempt by the vacancy pairs to avoid each other in the corresponding $\{111\}$ planes. Since the distortion of the regular fluorite structure around the vacancy pair is substantial, such a mutual avoidance may be seen simply as an attempt by the structure to minimize the strain. Off-setting this is the necessity to include the required percentage of vacancy pairs to achieve charge balance. It is interesting to compare the observed length-scale $1/r$ with the distance d defining the spacing of a perfectly regular packing of vacancy pairs on a triangular lattice necessary to achieve a given percentage of vacancies. The area per vacancy is $\frac{1}{2}\sqrt{3}d^2$ so that to achieve 2.5% of vacancy pairs in any one $\{111\}$ orientation $d = 6.8 \times \frac{1}{2}\langle 110\rangle$. This should be compared with the value $1/r = 4.7 \times \frac{1}{2}\langle 110\rangle$ seen in Fig. 5 corresponding to the value of $r = 0.3\mathbf{a}^*$ used in the syntheses. It might at first appear that the observed value for $1/r$, being considerably less than the theoretical maximum distance d, is suggesting that the vacancy pairs do not avoid each other as much as they might, but it must be borne in mind that we have assumed here that there is no interaction between vacancy pairs in one orientation with those in the other three orientations. This is unlikely to be the case in practice since, e.g., the present assumption of complete independence of the four different orientations means that some (albeit a small number of) cations will be surrounded by less than six oxygens. Further investigations of the constraints that this hypothetical mechanism might put on the distributions as a function of concentration are under way.

CONCLUSION

In this paper we have investigated the diffuse X-ray scattering patterns of example cubic stabilised zirconias (CSZs) from a modulation wave point of view. In this method it is assumed that the diffuse intensity in an elemental volume of the first Brillouin zone of reciprocal space arises from a periodic perturbation of the average real-space structure. Such a modulation may in practice be a complex combination of concentration variations and accompanying displacements, but in the present work we have used it in its simplest form, where only compositional variations are considered, to construct real-space distributions of oxygen vacancies. Displacements of atoms relaxing around the generated vacancies were obtained using the same simple algorithm that was previously reported (Welberry *et al.* (9)). In this it is assumed that cations move apart when either of the two bridging oxygen sites is vacant and correspondingly closer together when both are occupied.

The modulations that were used to synthesize the distributions consisted of all waves with wave vectors lying on a circle of radius r, centered at $\frac{1}{2}\{111\}^*$, in a plane normal to each of the four $\{111\}^*$ directions. When the waves were used to modulate the simple cubic array of oxygen sites the distribution of vacancies that resulted gave rise to relaxational displacements giving quite incorrect diffraction patterns. A second more successful set of syntheses was carried out in which the waves were used to modulate oxygen sites in pairs. That is, around any cation site the eight oxygen sites were considered as four

differently oriented and quite independent $\frac{1}{2}\langle 111\rangle$ pairs. It was assumed that modulations with wave vectors defined by one of the diffuse circles were caused by (and hence were descriptive of) the distribution of vacancy pairs in only one of the four possible orientations. Syntheses carried out in this way gave oxygen vacancy distributions having a correlation structure bearing a broad similarity to that obtained in the previous Monte Carlo study, and giving diffraction patterns equally convincingly like the observed ones.

The diffuse circles of scattering can be specified by only two parameters: the radius, r, which can be measured directly from the experiment and a degree of diffuseness which was defined in terms of the real-space distance over which the modulations were assumed to extend. By altering the latter quantity, σ_c, syntheses were carried out which gave rise to diffraction patterns which showed diffuse peaks ranging from fairly diffuse ones as found in the Y–CSZ example to much more peaked ones as found in the Ca–CSZ example.

Although the description of the disorder in terms of these two quantities is very simple and therefore perhaps useful in terms of categorizing different CSZs, there are a number of approximations inherent in the modulation wave synthesis method that warn against reading too much into the actual details of the description. What is most significant about the present work is the new insight that the method has given. As a result of the present work a new mechanism is suggested for the way in which the complex atomic arrangements in CSZs arise. This mechanism may be stated briefly as follows.

Vacancies occur as $\frac{1}{2}\langle 111\rangle$ pairs, providing octahedral coordination for a relatively small number of cations. When such a [6]-coordinated cation occurs the original cube of oxygen sites is distorted by extending the length of the cube-diagonal corresponding to the pair-direction and relatively contracting the directions normal to this to accommodate the valence requirements of the cation. Reference to the Table of preferred bond-distances for different coordination numbers given in Welberry *et al.* (8) indicates that for [6]-coordination Zr atoms prefer a bond distance of 2.078 Å compared with 2.241 Å for the corresponding distance in the *average* structure. This local distortion produces a strain field which extends out from the cation site to considerable distances isotropically in the plane normal to the pair direction. The strain field from one [6]-coordinated cation repels other similarly oriented [6]-coordinated cation sites, so that such defects tend to occur with a minimum separation distance between them in the corresponding {111} plane. The strain field in directions parallel to the pair direction can be dissipated almost immediately because the next cube in that direction is a vacant one. The present investigations seem to indicate that to a first approximation the strain fields associated with the differently oriented vacancy pairs do not interact greatly, but more extensive investigation of this possibility is required before this can be asserted with complete confidence. If it is assumed that differently oriented vacancy pairs do not repel each other then the possibility arises that neighboring $\frac{1}{2}\langle 110\rangle$ cation sites can share a vacancy to make a zigzag pair of octahedrally coordinated cations—a fairly frequently occurring feature in our earlier Monte Carlo model.

It is interesting to conjecture on the reasons for the different radii and degrees of diffuseness of the diffuse circles observed in the two different systems Ca–CSZ and Y–CSZ. For Y–CSZ even when the vacancy concentration is high (~10%) the diffuse rings are fairly broad but preliminary observations on samples of lower concentration indicate that they get even broader at lower concentrations. This seems to imply that the strain associated with a vacancy pair in this system is not great, allowing a great deal of variability in the spacing between pairs. For the Ca–CSZ system we so far have access to only one composition, corresponding to ~6.25% vacancies, and in this the circles are much more sharply defined. This seems to imply that the strain in this system is much higher, demanding a much tighter "zone of exclusion" with less variability.

On the other hand the radius of the circle observed for the (~6.25% vacancy) Ca–CSZ sample is somewhat larger than for the (~10% vacancy) Y–CSZ sample. This cannot be readily understood if, as we have assumed here, that only vacancy pairs of the same orientation repel each other in the appropriate {111} plane. It seems likely that for the Ca–CSZ system it will be necessary to consider interaction between the differently oriented pairs. It is interesting to note that the maximum vacancy concentration that can be obtained in Ca–CSZ is much less than that in Y–CSZ (5, 20).

Further work aimed at substantiating the viability of the above mechanism is in progress.

ACKNOWLEDGMENTS

We thank Dr. Brent Butler without whose program for the calculation of the diffuse diffraction patterns the present work would not have been possible. We also thank Joseph F. Wenckus, Chairman of Ceres Corporation, for the generous supply of single crystal samples used in this study. The diffuse scattering images shown in Figs. 3 and 4 were computed on a Fujitsu VP-2200 supercomputer using a grant from the Australian National University Supercomputer Facility.

REFERENCES

1. J. G. Allpress and H. J. Rossell, *J. Solid State Chem.* **15,** 68 (1975).
2. H. J. Rossell and H. G. Scott, *J. Phys. Colloque C7 no 12,* **38,** C7 (1977).
3. S. Hull, T. D. W. Farley, M. A. Hackett, W. Hayes, R. Osborn,

N. H. Andersen, K. Clausen, M. T. Hutchings, and W. G. Stirling, *Solid State Ionics* **28–30,** 488 (1988).
4. R. B. Neder, F. Frey, and H. Schultz, *Acta Crystallogr. A* **46,** 799 (1990).
5. H. J. Rossell, J. R. Sellar, and I. J. Wilson, *Acta Crystallogr. B* **47,** 862 (1991).
6. Th. Proffen, R. B. Neder, F. Frey, and W. Assmus, *Acta Crystallogr. B* **49,** 599 (1993).
7. Th. Proffen, R. B. Neder, F. Frey, D. A. Keen, and C. M. E. Zeyen, *Acta Crystallogr. B* **49,** 605 (1993).
8. T. R. Welberry, R. L. Withers, J. G. Thompson, and B. D. Butler, *J. Solid State Chem.* **100,** 71 (1992).
9. T. R. Welberry, B. D. Butler, J. G. Thompson, and R. L. Withers, *J. Solid State Chem.* **106,** 461 (1993).
10. T. R. Welberry and B. D. Butler, *J. Appl. Crystallogr.* **27,** 205–231 (1994).
11. T. R. Welberry and R. L. Withers, *J. Appl. Crystallogr.* **20,** 280 (1987).
12. T. R. Welberry and R. L. Withers, *J. Appl. Crystallogr.* **23,** 303 (1990).
13. T. R. Welberry, R. L. Withers, and J. C. Osborn, *J. Appl. Crystallogr.* **23,** 303 (1990).
14. B. D. Butler and T. R. Welberry, *J. Appl. Crystallogr.* **25,** 391 (1992).
15. B. D. Butler, R. L. Withers, and T. R. Welberry, *Acta Crystallogr. A* **48,** 737 (1992).
16. B. D. Butler and T. R. Welberry, *Acta Crystallogr. A* **49,** 736 (1993).
17. T. R. Welberry and R. L. Withers, *Phys. Chem. Miner.* **17,** 117 (1990).
18. B. D. Butler, T. R. Welberry, and R. L. Withers, *Phys. Chem. Miner.* **20,** 323 (1993).
19. T. R. Welberry and T. N. Zemb, *J. Colloid Interface Sci.* **123,** 413 (1988).
20. A. Rouanet, *Rev. Int. Hautes Temp. Refract.* **8,** 161 (1971).